International Journal of Nanomedicine

Dovepress
open access to scientific and medical research

Open Access Full Text Article

ORIGINAL RESEARCH

Tumor-targeting photodynamic therapy based on folate-modified polydopamine nanoparticles

This article was published in the following Dove Press journal:
International Journal of Nanomedicine

Shufeng Yan[1]
Qingqing Huang[1]
Jincan Chen[2]
Xiaorong Song[2]
Zhuo Chen[2]
Mingdong Huang[3]
Peng Xu[4]
Juncheng Zhang[1]

[1]Medical Plant Exploitation and Utilization Engineering Research Center, Sanming University, Sanming, Fujian 365004, People's Republic of China; [2]State Key Laboratory of Structural Chemistry, Fujian Institute of Research on the Structure of Matter, Chinese Academy of Sciences, Fuzhou, Fujian 350002, People's Republic of China; [3]College of Chemistry, Fuzhou University, Fuzhou, Fujian 350116, People's Republic of China; [4]Institute of Molecular and Cell Biology, A*STAR (Agency for Science, Technology and Research), Singapore 138673, Singapore

Background: Photodynamic therapy (PDT), a clinical anticancer therapeutic modality, has a long history in clinical cancer treatments since the 1970s. However, PDT has not been widely used largely because of metabolic problems and off-target phototoxicities of the current clinical photosensitizers.

Purpose: The objective of the study is to develop a high-efficiency and high-specificity carrier to precisely deliver photosensitizers to tumor sites, aiming at addressing metabolic problems, as well as the systemic damages current clinical photosensitizers are known to cause.

Methods: We synthesized a polydopamine (PDA)-based carrier with the modification of folic acid (FA), which is to target the overexpressed folate receptors on tumor surfaces. We used this carrier to load a cationic phthalocyanine-type photosensitizer (Pc) and generated a PDA-FA-Pc nanomedicine. We determined the antitumor effects and the specificity to tumor cell lines in vitro. In addition, we established human cancer-xenografted mice models to evaluate the tumor-targeting property and anticancer efficacies in vivo.

Results: Our PDA-FA-Pc nanomedicine demonstrated a high stability in normal physiological conditions, however, could specifically release photosensitizers in acidic conditions, eg, tumor microenvironment and lysosomes in cancer cells. Additionally, PDA-FA-Pc nanomedicine demonstrated a much higher cellular uptake and phototoxicity in cancer cell lines than in healthy cell lines. Moreover, the in vivo imaging data indicated excellent tumor-targeting properties of PDA-FA-Pc nanomedicine in human cancer-xenografted mice. Lastly, PDA-FA-Pc nanomedicine was found to significantly suppress tumor growth within two human cancer-xenografted mice models.

Conclusion: Our current study not only demonstrates PDA-FA-Pc nanomedicine as a highly potent and specific anticancer agent, but also suggests a strategy to address the metabolic and specificity problems of clinical photosensitizers.

Keywords: tumor-targeting, photodynamic therapy, folate receptors, polydopamine nanoparticles, anticancer specificity

Correspondence: Peng Xu
Institute of Molecular and Cell Biology, A*STAR (Agency for Science, Technology and Research), 61 Biopolis Dr, Singapore 138673, Singapore
Email xupeng@imcb.a-star.edu.sg

Juncheng Zhang
Medical Plant Exploitation and Utilization Engineering Research Center, Sanming University, 25 Jingdong Road, Sanming, Fujian 365004, People's Republic of China
Email 19900204@fjsmu.edu.cn

Introduction

Cancer is a global life-threaten disease, which brings about considerable suffering and burden to patients, as well as society as a whole. In the United States, the new incidence and mortality in 2019 are expected to be 1,762,450 and 606,880, respectively, corresponding to approximate 1700 deaths per day.[1,2] Traditional anticancer therapies, including surgical resections and chemotherapies, bring about severe systemic damages to patients. One main reason is that these approaches lack of sufficient specificity to tumor tissues, which leads to serious off-target damages on healthy organs.[3–5] Considerable efforts have been performed to develop novel

submit your manuscript | www.dovepress.com
DovePress
http://doi.org/10.2147/IJN.S216194

therapeutic strategies for cancers in the past decades. However, these new anticancer approaches show limited effects on relieving symptoms or enhancing survival rates in clinical settings. Thus, therapeutic strategies with higher specificity are desirable in order to achieve better anticancer outcomes.

Photodynamic therapy (PDT) is a clinical therapeutic modality for cancers by the illumination-induced generation of ROSs. With the appropriate illumination, photosensitizers in tumor sites produce cytotoxic ROSs to eradicate cancer cells. In addition to the transient generation of cytotoxic ROSs, increasing evidence demonstrate that PDT stimulates innate immune system, which further induces adaptive immune responses preventing the recurrence of cancer, leading to long-term antitumor effects.[6] Compared with traditional therapeutics (eg, surgical resections, radiotherapies or chemotherapies), PDT is a minimally invasive therapeutic approach with the properties of mild systemic toxicities, repeatable treatments, no drug-resistance, which remarkably enhances the life qualities and survival rates of patients. Besides, unlike the immunosuppressive nature of traditional anticancer therapeutics, PDT stimulates immune system of patients to facilitate cancer clearance.[7] PDT has been clinically used for the treatments of multiple types of cancer, including skin, esophagus, nasopharyngeal cancers, etc.[8–10] The concept of PDT for cancer treatments can be derived back to 1913, when German scientists used eosin with the combination of illumination to treat skin carcinoma. The first real modern clinical trial of PDT-based cancer therapy was in 1978, when haematoporphyrin derivativewas used for the treatments of cutaneous or subcutaneous cancers in New York.[11] However, over the last 40 years, very few photosensitizers have entered into clinical trials or have been approved for cancer therapies. This is in contrast to the massive researches which have been performed on the development of new photosensitizers. The slow translation of research into clinical applications is partially due to the off-target phototoxicities (skin burns) and the metabolic problems photosensitizers noted in clinical trials.[12–14] Using carriers to deliver photosensitizers has been considered to enhance the anticancer effects of PDT. Polymers in the nanometer-sizes are of considerable interests as carriers for small-molecule or peptide-based drugs. First, these carriers are of long circulating time and retention time in vivo, which improved the poor metabolic stability of small-molecule and peptide-based drugs caused by the fast renal clearance.[15–18] In addition, many nm-sized drug carriers remarkably improve the poor membrane permeability of small-molecule drugs, especially peptides. Furthermore, polymers ranged 100–200 nm have been reported to show excellent enhanced permeability and retention (EPR) effects in cancer mice models, which leads to the more reasonable biodistributions and passive tumor-targeting properties.[19,20]

A large number of polymers have been used for drug delivery to prolong the in vivo retention time of small-molecule drugs. One of the most widely studied drug carrier is polyethylene glycol (PEG), which has been used to modify various FDA-approved drugs.[21] However, recent studies have demonstrated that PEG caused reduced cellular uptake, eliciting immune responses, non-specific binding to blood proteins, etc.[22] In addition to PEGs, many other efforts have been performed to deliver photosensitizers or other anticancer agents to the tumor sites.[23–26] Increasing evidence suggest that polydopamine (PDA) as a promising drug carrier because of its natural composition, excellent biocompatibility, non-toxicity, non-immunogenicity, non-antigenicity and high solubility in aqueous solutions.[27–30] PDA shows high potency to load multifarious biomolecules, and effectively enhances the pharmaceutical effects of therapeutics.[31–33] Meanwhile, PDA is prone to release the loaded drugs in the acidic tumor microenvironments or lysosomes, because PDA nanoparticles have been reported to rapidly disintegrate at low pH.[34–36] Cancer development involves a large number of specific signaling pathways, which requires the overexpression of specific membrane-bound receptors for accommodating relevant ligands. Compared to healthy cells, multiple tumor cells express high levels of folate receptors (FRs) on their surface, which have been identified as promising diagnostic and therapeutic targets for cancers.[37,38] Patients bearing FRs-positive tumors have shown better clinical outcomes with the FRs-targeting treatments than patients bearing FR-negative tumors.[39,40] Thus, targeting FRs is considered as an effective approach to improve the tumor-targeting properties of anticancer drugs.[41,42] Folic acid (FA) is one of the best-characterized ligands with high affinity to FRs ($KD<10^{-9}$ M) and has been exploited to enhance the drug internalization into tumor cells through the FR-mediated endocytosis.[43–49] Besides, FA-conjugated nanoparticles have demonstrated excellent diagnostic and therapeutic potencies in experimental cancer models.[50–54]

In this study, to address the metabolic problems and promoting the insufficient tumor-targeting properties of clinical photosensitizers, we used a FA-modified PDA

nanocarrier loading a phthalocyanine-based photosensitizer to target the peri-cellular FRs on tumor cells. In our previous study, we reported a highly positive zinc phthalocyanine-type photosensitizer, $ZnPc(TAP)_4^{12+}$, which is referred to as Pc in the flowing text. Pc is a zinc phthalocyanine derivative with four 2,4,6-tris (N, N-dimethylaminomethyl) phenoxyl (TAP) moieties modified in the four margins (Figure S1). With the methylations of the 12 tertiary amines, Pc contained 12 positive charges in one photosensitizer molecule, which was able to attach the negatively charged PDA surface via electrostatic attractions. Pc demonstrated high potency as the anticancer agent owing to its fine water-solubility, photostability and high ROSs generation yield.[55,56] This PDA-based nanomedicine (PDA-FA-Pc) can be disintegrated in the acidic tumor microenvironment or lysosomes and release the photosensitizer (Pc) to eliminate cancer cells. The synergistic effects of PDA and FA will significantly improve the anticancer efficacies and specificities of Pc in vitro and in vivo. Furthermore, our PDA-FA-Pc nanomedicine demonstrated remarkable selective photodynamic effects to the FR-overexpressing cancer cell lines, suggesting the excellent anticancer effects and safety in cancer treatments.

Materials and methods

Materials

All chemicals including dopamine hydrochloride, FA, 2,4,6-tris (N, N-dimethylaminomethyl) phenoxy (TAP), MTT and DAPI were purchased from Sigma-Aldrich (St. Louis, USA) or Sinopharm Chemical Reagent Co. Ltd. (Shanghai, People's Republic of China). All chemicals were of analytical grade and used without further purification unless notified. Human cervical carcinoma cell line Hela, human breast adenocarcinoma cell line MCF-7, human embryonic lung fibroblast HELF and human normal liver cell L02 were purchased from the China Center for Type Culture Collection. The cells were maintained in DMEM or RPMI-1640 medium supplemented with 10% FBS, 100 U/mL penicillin and 100 mg/mL streptomycin (Gibco, Invitrogen, Grand Island, NY, USA) at 37°C with 5% CO_2.

Preparation of PDA

PDA nanoparticles were synthesized through the oxidative-polymerization of dopamine hydrochloride following our previously established protocol with an average diameter of 160–170 nm.[30] In brief, 1 mL NH_4OH (28–30%) was mixed with 20 mL ethanol and 45 mL deionized (DI) water under stirring for 30 mins at room temperature. 250 mg dopamine hydrochloride was dissolved in 5 mL DI water and then injected into the above-mixed liquors. The color of the mixed liquors turned pale yellow immediately and then gradually changed to dark brown. The mixed liquors were then allowed to stand overnight. PDA was collected after centrifugation, washing and re-dispersing with DI water, until no color in the supernatant was observed.

Preparation of $ZnPc(TAP)_4^{12+}$ (Pc)

The photosensitizer used in this study ($ZnPc(TAP)_4^{12+}$, Pc) was synthesized as previously reported, and the chemical structure was presented in Figure S1, which was slightly modified from our approach previously reported.[55] In brief, $ZnPc(TAP)_4$ (166 mg, 0.1 mmol) dissolved in DMF (100 mL) was stirred with CH_3I (86 μL, 1.35 mmol) for 6 hrs at room temperature leading to the positively charged ZnPc $(TAP)_4^{12+}$, which showed excellent aqueous solubility (>10 mg/mL in water). Then, the mixture was concentrated to 10 mL by removing the solvent under reduced pressure. The product was precipitated upon the addition of diethyl ether to the residue and the precipitates were collected by centrifugation (dissolved in methanol). Thereafter, the insoluble impurities were filtered off and the filtrate was precipitated by diethyl ether again. Finally, the product was centrifuged and dried in a vacuum to yield the $ZnPc(TAP)_4^{12+}$.

Synthesis of PDA-FA-Pc nanomedicine

The design and synthetic strategy of PDA-FA-Pc nanomedicine has been illustrated in Figure 1A. The PDA-FA was prepared firstly before loading Pc. The FA was dissolved in Tris-HCl (Tris(hydroxymethyl)aminomethane-HCl) solution with a concentration of 0.5 mg/mL. Although the solubility of FA in neutral water is relatively low, it dissolves well in weak basic Tris-HCl buffer solution. Next, 50 mg PDA nanoparticles were added and dispersed in Tris-HCl solution by stirring. The mixed solution was stirred at room temperature for 2 hrs. After reaction, the product was centrifuged and washed with DI water. For loading Pc, the PDA-FA solution (1 mg/mL) was mixed with excess Pc and stirred for another 2 hrs. Unbound Pc was completely removed by centrifugal filtration. The obtained PDA-FA-Pc nanomedicine was readily dispersed in water, forming solutions with dark brown color resembling the PDA solution. PDA-FA-Pc nanomedicine was re-suspended in DI water and stored at 4°C for subsequent experiments. The degree of loading (DOL) of FA or Pc in PDA-FA-Pc nanomedicine was determined based on the

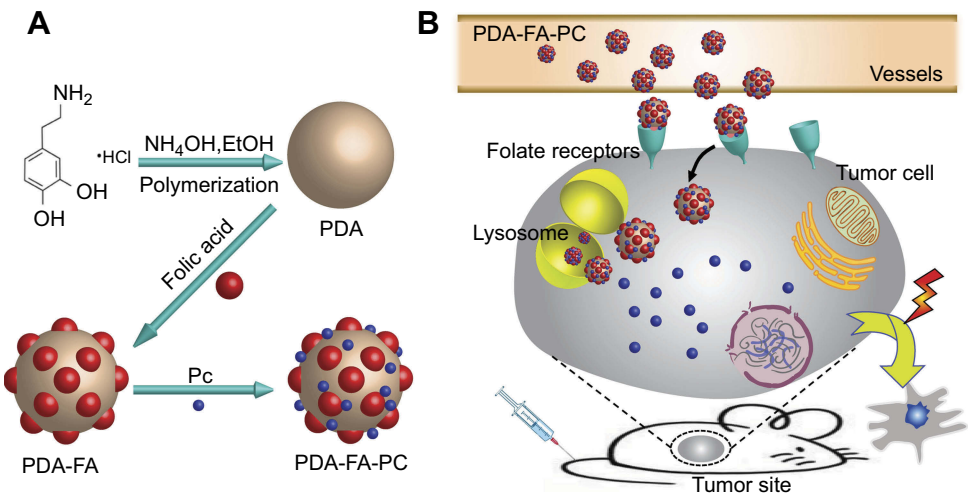

Figure 1 (**A**) The synthetic scheme of PDA-FA-Pc nanomedicine. (**B**) The illustration of the anticancer mechanism of PDA-FA-Pc nanomedicine: After intravenous injection, PDA-FA-Pc nanomedicine crosses the vascular wall and accumulates in tumor tissues via EPR effects and targeting the FRs on tumor cell surfaces. In the relative acidic tumor microenvironment or lysosomes after internalization, PDA-FA-Pc nanomedicine disintegrates and releases monomeric Pc molecules, which exhibit photodynamic effects to eradicate tumor cells.

specific absorbance (360 nm for FA and 690 nm for Pc) of PDA-FA or PDA-FA-Pc. The loading amount of FA or Pc on PDA-FA-Pc nanomedicine (mg) was calculated according to the standard curves derived from the absorbance of pure FA or Pc. The DOL was calculated according to the following equation: DOL (%)=(weight of FA or Pc)/(weight of PDA-FA-Pc nanomedicine)×100%. For Pc releasing measurement, PDA-FA-Pc nanomedicine solutions were dialyzed in phosphate buffers at pH 5 and 7 in dark. At different time points (2, 4, 8 and 16 hrs), Pc released from PDA-FA-Pc nanomedicine was collected and calculated based on the standard curve derived from the absorption spectrum of pure Pc.

Characterization of PDA-FA-Pc nanomedicine

The morphology of the sample was investigated by a JSM 6700F scanning electron microscope . The UV-vis absorption spectrum of PDA-FA-Pc nanomedicine at 10 mg/mL in DI water was measured by Synergy 4 multi-mode microplate reader (BioTek Instruments, USA). The HD distribution and zeta potentials of PDA-FA-Pc nanomedicine were determined by dynamic light scattering (DLS) measurement (Nano ZS90, Malvern Instruments, UK). To study the stability of PDA and PDA-FA-Pc, we let them stand in PBS at room temperature and investigated the size changes during 8 days. For the dispersibility, we dispersed PDA-FA-Pc in H_2O, PBS, PBS+20% FBS and let them stand for 24 hrs at room temperature. The data curves were fitted to exponential functions using Origin and Prism-5 software.

Determination of ROS generation

The production of ROS by PDA-FA-Pc nanomedicine was measured with the 2,7-dichlorofluorescein diacetate (DCFH-DA) as a probe of ROS. To specify, 10 μM DCFH-DA was incubated with PDA-FA-Pc nanomedicine at various concentrations (0.15, 0.3, 0.6, 1.2 and 2.4 mg/mL) in PBS, and illuminated by a planar LED light source (2.5 J/cm^2, 680 nm). The control group without PDA-FA-Pc nanomedicine treatment was measured for comparison. Finally, the fluorescence change of ROS probe was determined by a BioTek microplate reader at the excitation wavelength 488 nm and emission wavelength 525 nm after incubation for different periods.

Cellular uptake studies

For cellular uptake studies, a suspension of Hela, MCF-7, HELF and L02 cells were plated in 96-multiwell plates, respectively (5×10^4/mL, 200 μL/well), and keep overnight at 37°C under 5% CO_2. After incubation of 1, 2 and 4 hrs with PDA-FA-Pc nanomedicine (2 mg/mL), all cells were gently rinsed with PBS to remove redundant agents. Cells were lysed (0.1 M NaOH, 1% SDS) to give a homogeneous solution and the fluorescence of cell lysates was measured by Synergy 4 multi-mode microplate reader (λ_{ex}=610 nm, λ_{em}=692 nm). Protein concentration of cells were determined by Pierce™ BCA Protein Assay

Kit (BioTek Corporation, People's Republic of China) and expressed as nmol phthalocyanine per mg cellular proteins (nmol/mg). The control wells in the plate with only culture medium serve as a blank. To further evaluate the cellular uptake of PDA-FA-Pc nanomedicine in Hela, MCF-7, HELF and L02 cells, we investigated cellular uptake by flow cytometry (Beckmann Corporation, USA). A suspension of Hela cells, MCF-7 cells, HELF cells and L02 cells (5×10^4/mL, 2 mL/well) were plated onto 6-well plates, respectively. All cells were treated with PDA-FA-Pc nanomedicine (2 mg/mL) for 2 h after adhesion. Thereafter, cells were washed carefully with PBS, collected and analyzed by flow cytometry. The control cells in the plate with only culture medium serve as control group.

Sub-cellular localization of PDA-FA-Pc nanomedicine

For sub-cellular localization studies, the Hela, MCF-7, HELF and L02 cells (5×10^4/mL, 2 mL) were plated onto confocal chamber slides, respectively, and kept at 37°C overnight to adhesion. Then, the cell culture mediums containing PDA-FA-Pc nanomedicine at a concentration of 1 mg/mL were added. After 2-hr incubation, cells were gently washed by PBS to remove unbound PDA-FA-Pc nanomedicine. Afterward, at room temperature, all cells were fixed for 10 mins in using Immunol Staining Fix Solution. Subsequently, these cells incubated with 500 μL DNA fluorescent dye DAPI (5 μg/mL) for 5 mins. Finally, cells were washed by PBS thoroughly before being mounted for direct confocal microscopic observation (Olympus FluoView™ FV1000, Japan). The following filters were used for DAPI and PDA-FA-Pc nanomedicine: $359_{Ex}/461_{Em}$ for DAPI and $610_{Ex}/692_{Em}$ for PDA-FA-Pc nanomedicine.

In vitro cytotoxicity

The methyl thiazolyltetrazolium (MTT) assays were performed to investigate the in vitro phototoxicity and dark toxicity of PDA-FA-Pc nanomedicine for Hela, MCF-7, HELF and L02 cells. Briefly, cells were seeded into 96-well culture plates at a density of 1×10^4/well. Cells were attached after 16 hrs. All cells adhered to the bottom after 16 hrs and followed by incubation with PDA-FA-Pc nanomedicine at different concentrations (0.15, 0.3, 0.6, 1.2 and 2.4 mg/mL) for 2 hrs. Unbound PDA-FA-Pc nanomedicine was removed by washing in PBS thoroughly. Then, the cells of phototoxicity groups were followed by 2-min illumination at a dose of 5 J/cm^2 via a planar LED light source (680 nm) and incubation of 24 hrs. Next day, cells in each well were mixed with 100 μL of 0.5 mg/mL MTT solution in cell culture medium and incubated for 4 hrs. The formed insoluble purple formazan product was then dissolved in DMSO (100 μL each well). The absorbance of the solution was quantified by measuring at 570 nm with a Synergy 4 multi-mode microplate reader. Meanwhile, dark toxicity experiments of PDA-FA-Pc nanomedicine for all cells were also investigated without illumination.

Phototoxicity of PDA-FA-Pc nanomedicine with the competition with FA

The phototoxicity of sole FA was determined in the same way as that of PDA-FA-Pc nanomedicine in Hela cells. For competition experiment, cells were seeded into 96-well culture plates at a density of 1×10^4/well. After adhesion, cells were pre-incubated with 0.4 μg/mL sole FA followed by incubation with 0.6 mg/mL PDA-FA-Pc nanomedicine for 1, 2 and 4 hrs. The survival rates of Hela cells were determined by the MTT assays.

Establishment of HeLa and MCF-7 tumor-bearing mouse models

Female Kunming mice (4 weeks old, 20 g, purchased from Shanghai SLAC Laboratory Animal Co. Ltd., People's Republic of China). All experiments were performed following the guidelines of the institutional animal care and use committee of Fujian Institute of Research on the Structure of Matter, Chinese Academy of Sciences. The committee also approved the experiments. Shufeng Yan had received training under the ethical approval of Fujian Institute of Research on the Structure of Matter, Chinese Academy of Science. During experiments, all mice were allowed free access to water and food. To establish the Hela and MCF-7 tumor-bearing mouse models, 0.2 mL suspension of Hela or MCF-7 cells in sterilized saline with a density of 1.0×10^7 cells/mL were subcutaneously inoculated into the right flank of Kunming mice, respectively. The therapy experiment started when the tumor size reached 50 mm^3 (Hela tumor-bearing mice) or 35 mm^3 (MCF-7 tumor-bearing mice), typically 5 days after inoculation.

Fluorescent molecular tomography (FMT) imaging of PDA-FA-Pc nanomedicine in MCF-7 tumor-bearing mice

The MCF-7 tumor-bearing mice model was established with the equivalent average starting tumor size (100–150 mm^3) and body weight (~23 g). The mice were injected with PDA-FA-Pc nanomedicine (43.5 mg/kg of total mouse body weight) intravenously via the caudal vein. After injection, mice were anesthetized using inhaled isoflurane and placed in an imaging cassette to be imaged using a fluorescent molecular tomography FMT 2500^{TM} LX instrument. The tumor-targeting capability of PDA-FA-Pc nanomedicine within the mice was monitored at different time points (3, 6, 12, 24, 48 and 96 hrs). All FMT scans were carried out using a 680 nm laser diode which was used to excite the ZnPcs and long wavelength fluorescence emission (690–740 nm) was detected. The regions of interest (ROIs) were scanned with 40–60 source locations and right scan parameters (~10,000 counts per pixel and 3 mm spacing between adjacent source locations). The imaging results were analyzed with the software TrueQuant v3.0 (PerkinElmer, Waltham, MA, USA) to derive quantitative information in terms of average concentrations of ZnPcs by creating ROIs around the tumor sites (T) and non-tumor sites.

In vivo antitumor efficacy

The antitumor effects of PDA-FA-Pc nanomedicine in Hela and MCF-7 tumor mice were evaluated by growth inhibition and tumor weight analysis. Typically, Hela and MCF-7 tumor-bearing mice (established as above) were randomly divided into PDA-Pc treated group, PDA-FA-Pc nanomedicine treated group and saline group, respectively (8 mice per group). Each mouse showed equivalent average starting tumor size (50 mm^3 for Hela tumor-bearing mice, 35 mm^3 for MCF-7 tumor-bearing mice) and body weight (~23 g). The mice of PDA-Pc treated group and PDA-FA-Pc nanomedicine treated group were treated by PDA-Pc and PDA-FA-Pc nanomedicine, respectively (43.5 mg/kg of total mouse body weight) via the caudal vein injection. The mice of saline group were injected intravenously with equivalent volume of saline as a control group. Twelve hours later, the tumor sites were illuminated with 680 nm light for 10 mins (a total light dose of 75 J/cm^2, LumaCare non-coherent light source, Luma Care Medical Group, Newport Beach, CA, USA). The body weights of mice were monitored daily and the tumor sizes were calculated with a caliper throughout the experiment using the ellipsoid volume formula $(W^2 \times L) \times \pi/6$, where W means tumor width and L means tumor length. After 8-day treatment, the mice were sacrificed, and their tumors were carefully dissected out for weight analysis.

Statistical analysis

All data represent group means and standard errors of the mean (SEM). The experimental data in vitro and in vivo were analyzed by two-way ANOVA. Differences at the 95% confidence level ($p<0.05$) were considered statistically significant.

Results and discussion

Design, synthesis and characterization

The design and synthesis of PDA-FA-Pc nanomedicine is illustrated in Figure 1A. Figure 1B elucidates the anticancer mechanism of PDA-FA-Pc nanomedicine. First, after intravenous injections, PDA-FA-Pc nanomedicine in vessels rapidly accumulates in tumor sites through the combination of the EPR effects and FA-FRs interaction. PDA-FA-Pc nanomedicine then disintegrates and releases Pc in the acidic tumor microenvironment or in lysosomes after endocytosis. The released Pc molecules in cytoplasm then exhibit photodynamic effects to cause the apoptosis and necrosis of cancer cells.

The obtained PDA-FA-Pc nanomedicine was characterized by scanning electron microscopy, DLS, UV-vis absorption spectra, etc. First, we used scanning electron microscopy to study the morphology of PDA-FA-Pc nanomedicine (Figure 2A). In scanning images, the fabricated PDA-FA-Pc nanomedicine showed homogeneous spherical configurations with an average diameter of 170 nm. The hydrodynamic diameter (HD) of PDA-FA-Pc nanomedicine was in the range of 160–180 nm determined by DLS analysis (Figures 2B and S2), consistent with the diameters determined by scanning electron microscopy. Figures 2A and B. In addition, non-measurable size change was observed during the 8 days (Figure S3), indicating the assembly configuration of PDA and PDA-FA-Pc was stable. Meanwhile, the PDA-FA-Pc nanomedicine exhibited high stability from disintegration or aggregation in aqueous solutions, like water, PBS or 20% FBS (Figure S4). Notably, nanoparticles in this size are reported to avoid the fast renal clearance in circulation system and high EPR effects in tumor sites.[57,58] The average HD of

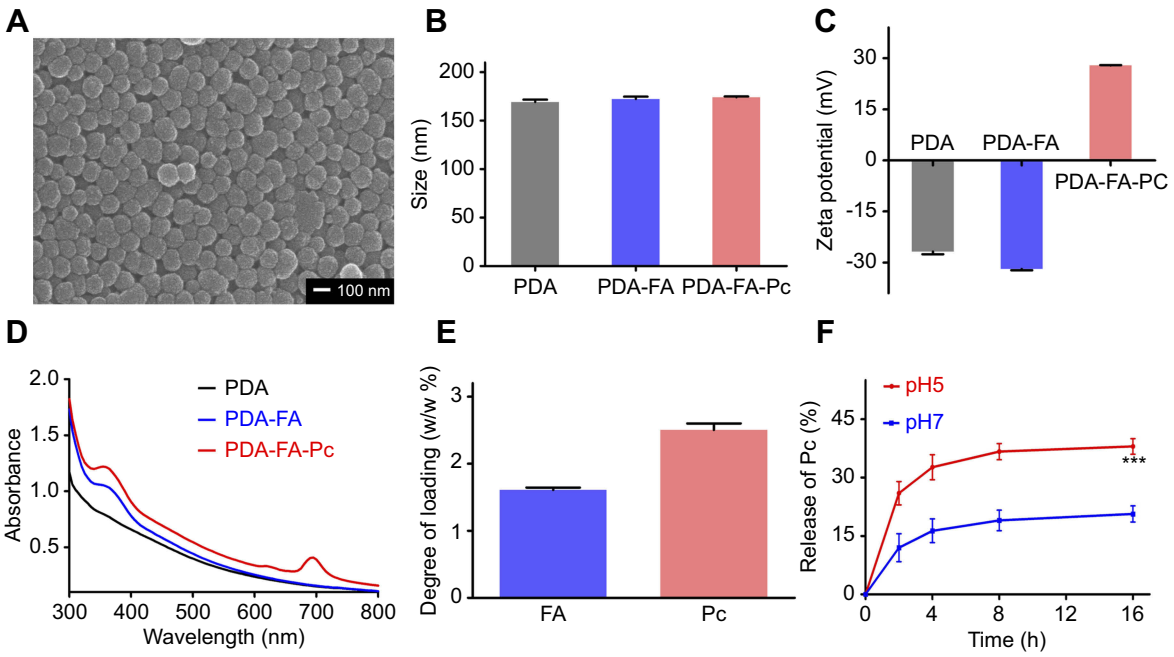

Figure 2 Characterization of PDA-FA-Pc nanomedicine. (**A**) The scanning electron microscopy image of PDA-FA-Pc nanomedicine. (**B**) The size distributions of PDA, PDA-FA and PDA-FA-Pc nanomedicine in water measured by DLS. (**C**) Zeta potentials of PDA, PDA-FA and PDA-FA-Pc nanomedicine. (**D**) UV-vis absorption spectra of PDA, PDA-FA and PDA-FA-Pc nanomedicine. The UV-vis absorption spectra of pure FA and Pc were shown in Figure S3. (**E**) The degree of loading (DOL) of FA and Pc in PDA-FA-Pc nanomedicine (w/w %). (**F**) The release of the monomeric Pc molecules from PDA-FA-Pc nanomedicine in acidic (pH 5) and neutralized (pH 7) conditions. The values were represented as mean ± SD, ***p <0.001.

PDA-FA-Pc nanomedicine was close to the HDs of PDA and PDA-FA. However, the zeta potential data showed that PDA-FA-Pc nanomedicine is generally positively charged in contrast to negative charged PDA and PDA-FA (Figure 2C), indicating the successful loading of the highly positive Pc. Notably, because of the overexpressed sialic acids, tumor cells normally are in a negative tumor microenvironment,[59] indicating that agents with positive charges, eg, PDA-FA-Pc nanomedicine, are favorable to penetrate into tumor tissues. In addition, the UV-vis absorption spectra also indicate the same information (Figures 2D and S5): PDA-FA-Pc nanomedicine showed obviously enhanced absorption at 360and 690 nm in contrast to PDA indicating the loading of FA and Pc, respectively.

We then determined the DOL of FA and Pc in PDA-FA-Pc nanomedicine. The DOLs of FA and Pc were quantified as 1.6% and 2.5% (w/w), respectively (Figure 2E). The antitumor efficacy of PDA-FA-Pc nanomedicine was mainly dependent on the PDT effect of Pc. We thus further investigated the release of Pc from PDA-FA-Pc nanomedicine in PBS at acidic (pH 5) and neutralized (pH 7) conditions (Figure 2F). The quantification of the released Pc was through determining the characteristic absorbance at 690 nm.[55] The Pc release in the acidic condition was much faster than that in the neutral condition, which was likely due to the faster disintegration of PDA nanomedicine at low pH solutions.[60] Notably, the maximum release rate in acidic condition (approximately 40%) was also significantly higher than that in neutralized condition (approximately 18%). The pH-dependent Pc release of PDA-Pc was further investigated and showed similar result with that of PDA-FA-Pc, indicating that FA did not affect the drug release of our PDA-based nanocarrier (Figure S6). The result indicates that PDA-FA-Pc nanomedicine is stable in circulation systems with neutralized conditions, while rapidly releases Pc in tumor microenvironments, endosomes and lysosomes in tumor tissues with acidic pH values. Such pH-sensitive drug releasing property of PDA-FA-Pc nanomedicine might achieve precisely controlled PDT effects in tumor tissues, which is able to minimize the systemic damages during delivery. In addition, the production of ROS by PDA-FA-Pc with illumination at 680 nm was further investigated by using DCFH-DA as the ROS probe. The result showed that PDA-FA-Pc nanomedicine induced significantly increased ROS release compared to the control group (Figure S7).

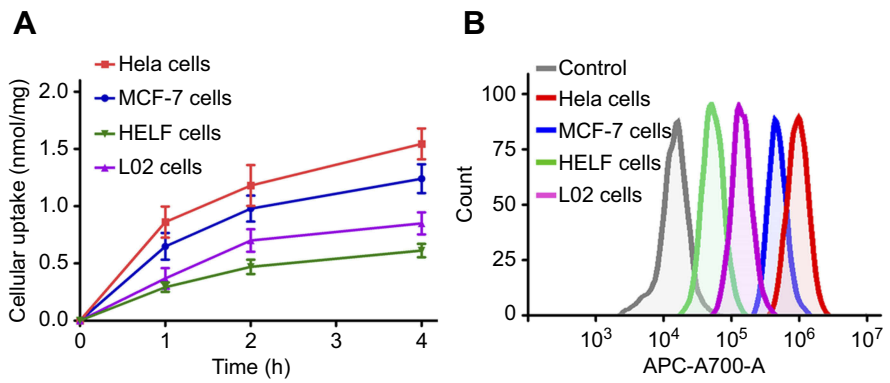

Figure 3 Cellular uptakes of PDA-FA-Pc nanomedicine in FRs overexpressed tumor cell lines (Hela, MCF-7) and healthy cell lines (HELF, L02) by fluorescence analysis (**A**) and flow cytometric analysis (**B**).

PDA-FA-Pc nanomedicine specifically recognized tumor cells

As many tumor cell lines overexpress membrane-anchored FRs on surface, we next evaluated whether our PDA-FA-Pc nanomedicine was able to specifically recognize FRs overexpressed tumor cell lines. Human cervical cancer cell line, Hela and human breast cancer cell line, MCF-7, have been reported to express excessive peri-cellular FRs. In addition, two healthy cell lines, human embryo lung fibroblasts (HELF) and human normal liver cells (L02), were set for comparison. The amount of Pc internalized in cells was quantified either through traditional fluorescence analysis (Figure 3A) and flow cytometric analysis (Figure 3B). As shown in Figure 3A, PDA-FA-Pc nanomedicine demonstrated time-dependent uptake in all the four cell lines. But approximate 2–4-fold faster and higher cellular uptake was observed in the two tumor cell lines in contrast to the uptake in the two healthy cell lines. Similar results were observed in the data of flow cytometric analysis (Figure 3B). The FR overexpressed tumor cell lines (Hela, MCF-7) showed significantly higher drug uptakes than healthy cells (HELF, L02) did, indicating that PDA-FA-Pc nanomedicine is able to recognize the FR on tumor surfaces and release Pc for photodynamic treatments.

Sub-cellular localization of PDA-FA-Pc nanomedicine

We then evaluated the sub-cellular localization of PDA-FA-Pc nanomedicine in FR overexpressed tumor cell lines (Hela, MCF-7) and healthy cell lines (HELF, L02) through confocal microscopy (Figure 4). The confocal images were captured after 2-hr incubation with PDA-FA-Pc nanomedicine. The Pc fluorescence had no overlap with the DAPI fluorescence, indicating that Pc did not penetrate the nuclei membranes avoiding gene

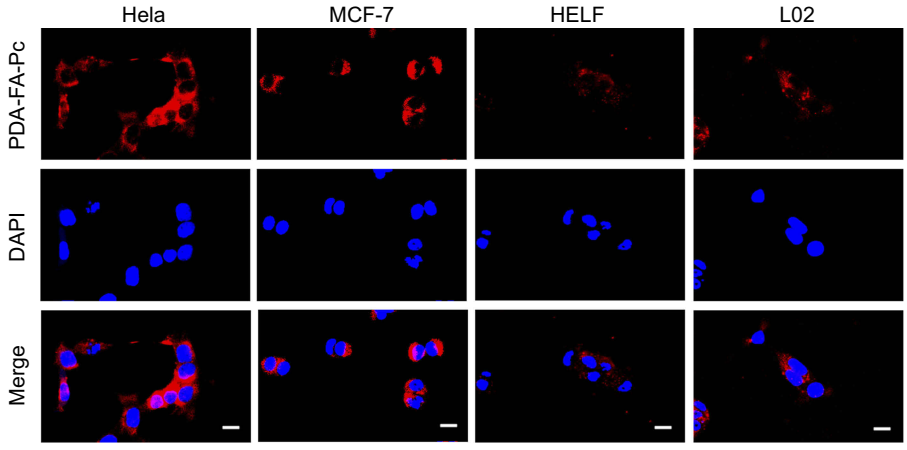

Figure 4 Subcellular imaging of PDA-FA-Pc nanomedicine in tumor cell lines (Hela and MCF-7) and healthy cell lines (HELF and L02). The fluorescent signals of DAPI (a dye for nuclei) and Pc were represented in blue and red, respectively. Scale bars represent 20 μm.

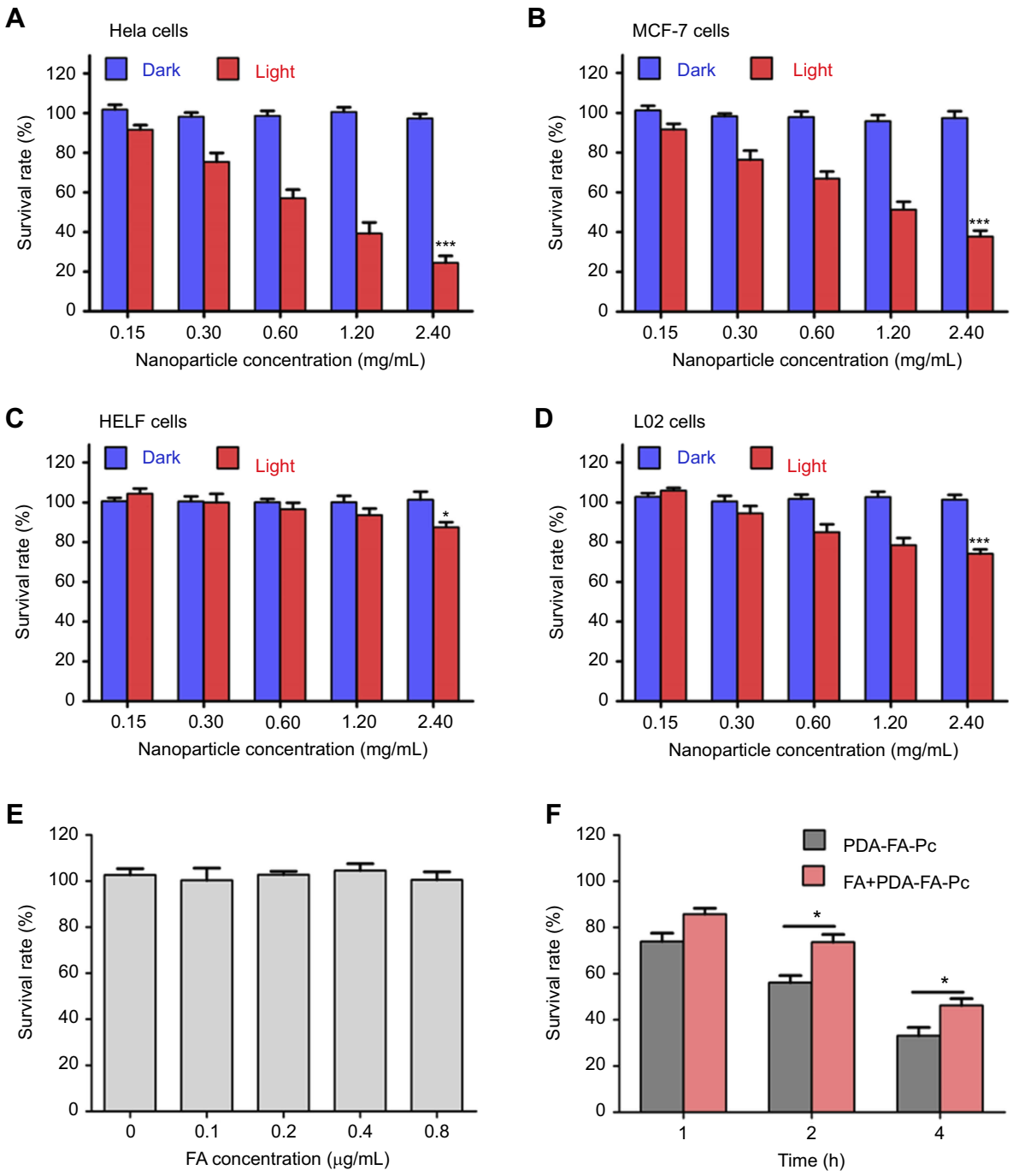

Figure 5 . Anticancer effects of PDA-FA-Pc nanomedicine in vitro. The survival rates of Hela (**A**), MCF-7 (**B**), HELF (**C**) and L02 cells (**D**) were determined after incubation with PDA-FA-Pc nanomedicineat various concentrations with and without illumination. (**E**) Phototoxicity of sole FA to Hela cells; (**F**) Time course for phototoxicities of PDA-FA-Pc nanomedicine (0.6 mg/mL) to Hela cells with and without competition with excessive FA (0.4 μg/mL). Phototoxicities were determined with the illumination at 680 nm with the light dose of 5 J/cm^2. The values were represented as mean ± SEM, *p<0.05, ***p<0.001 vs the vehicle (non-treated) group.

damages. In addition, the fluorescence of Pc was merely observed in the cytoplasm of healthy cells (HELF and L02). In contrast, at the same excitation voltage, the two tumor cell lines (Hela and MCF-7) showed intensive Pc fluorescence in cytoplasm, suggesting that the FA-FR interactions significantly enhanced the internalization of PDA-FA-Pc nanomedicine. The sub-cellular imaging result was consistent with the results of the cellular uptake assays, suggesting that the photosensitizer was released after the endocytosis of PDA-FA-Pc nanomedicine, and the Pc release occurred in organelles with low pH, eg, endosome and lysosome.

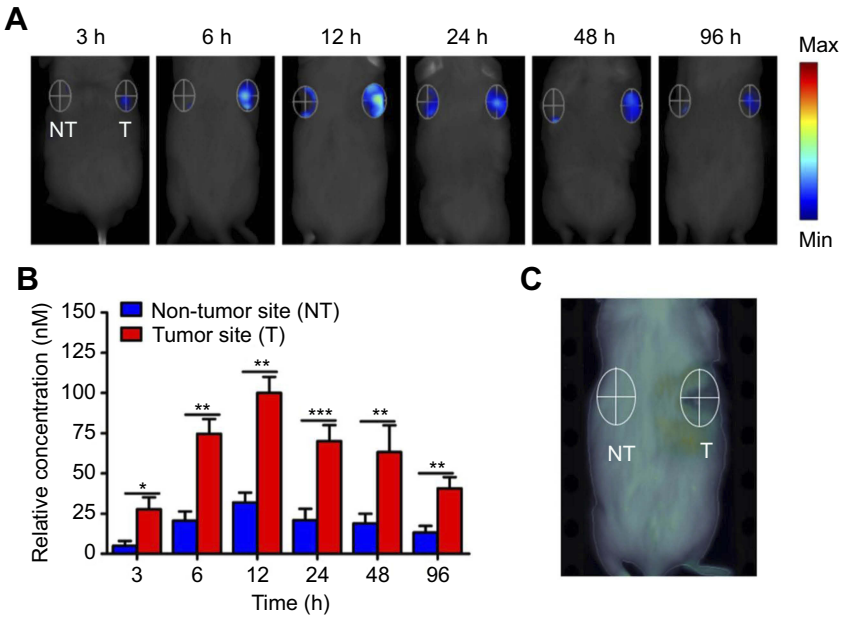

Figure 6 In vivo imaging of PDA-FA-Pc nanomedicine by fluorescent molecular tomography (FMT) imaging of Pc fluorescence in MCF-7 tumor-bearing mice. (**A**) Imaging graphics of PDA-FA-Pc at the tumor site (T, right) and non-tumor site (NT, left) at 3, 6, 12, 24, 48, and 96 h after intravenious injection. (**B**) Quantitations of Pc relative concentrations at the non-tumor (NT) and tumor sites (T) at different time points in panel a. (**C**) The non-tumor (NT) and tumor sites (T) of the saline treated mice showed non-measurable Pc fluorescence signal. The values were represented as mean ± SEM, ***p<0.001, **p<0.01, *p<0.05 vs the fluorescence signals at the NT site.

PDA-FA-Pc nanomedicine demonstrated specific photodynamic effects to cancer cell lines

Given the promising cellular uptake and sub-cellular localization of PDA-FA-Pc nanomedicine, we next evaluated the anticancer effects and the safety to healthy cells of our PDA-FA-Pc nanomedicine in vitro. We thus determined the phototoxicities and dark toxicities toward the FR overexpressed tumor cell lines (Hela, MCF-7) and healthy cell lines (HELF, L02). All above cells were treated with PDA-FA-Pc nanomedicine at the concentrations of 0.15, 0.3, 0.6, 1.2 and 2.4 mg/mL for 2 hrs followed by the assessment of the survival rates via MTT assays (Figure 5). In all cell lines, treatments with PDA-FA-Pc nanomedicine demonstrated non-measurable toxicity without illumination, suggesting the safety of avoiding off-target photodynamic effects. In contrast, PDA-FA-Pc nanomedicine demonstrated the dose-dependent phototoxicities of all the four cell lines with the light dosage of 5 J/cm^2 via a planar LED light source (680 nm). However, the phototoxicities of PDA-FA-Pc nanomedicine to the two tumor cell lines were much more significant than those in the two healthy cell lines, consistent with the much higher cellular uptakes above. The higher phototoxicities of our PDA-FA-Pc nanomedicine in tumor cells were likely due to the specificity to the FR on tumor surfaces. In addition, no phototoxicity was observed when Hela cells were treated with PDA or PDA-FA (Figure S8), indicating that the photodynamic activity of PDA-FA-Pc nanomedicine was mainly attributed to the Pc moiety.

FA competed down the phototoxicity of PDA-FA-Pc nanomedicine to tumor cells in vitro

To further verify the specificity of PDA-FA-Pc nanomedicine to the peri-cellular FRs, we determined a time-dependent phototoxicity of PDA-FA-Pc nanomedicine to Hela cells with and without the competition with excessive FA. First, we confirmed that FA had no photo- or dark-toxicity to tumor cells (Figure 5E). With the pre-incubation with 0.4 μg/mL FA, the phototoxicity of PDA-FA-Pc nanomedicine at 0.6 mg/mL was obviously reduced (Figure 5F) at all time points, indicating that the blockage of the pericellular FRs obstructed the accumulation of PDA-FA-Pc nanomedicine on tumor cell surface. However, excessive FA only partially competed down the phototoxicity of PDA-FA-Pc nanomedicine, which might be explained by the fact that the released positively charged Pc monomers accumulated on the negatively charged tumor cell surface or passively crossed cell membranes. These data indicate that the antitumor effect of PDA-FA-Pc nanomedicine was partially FRs-mediated.

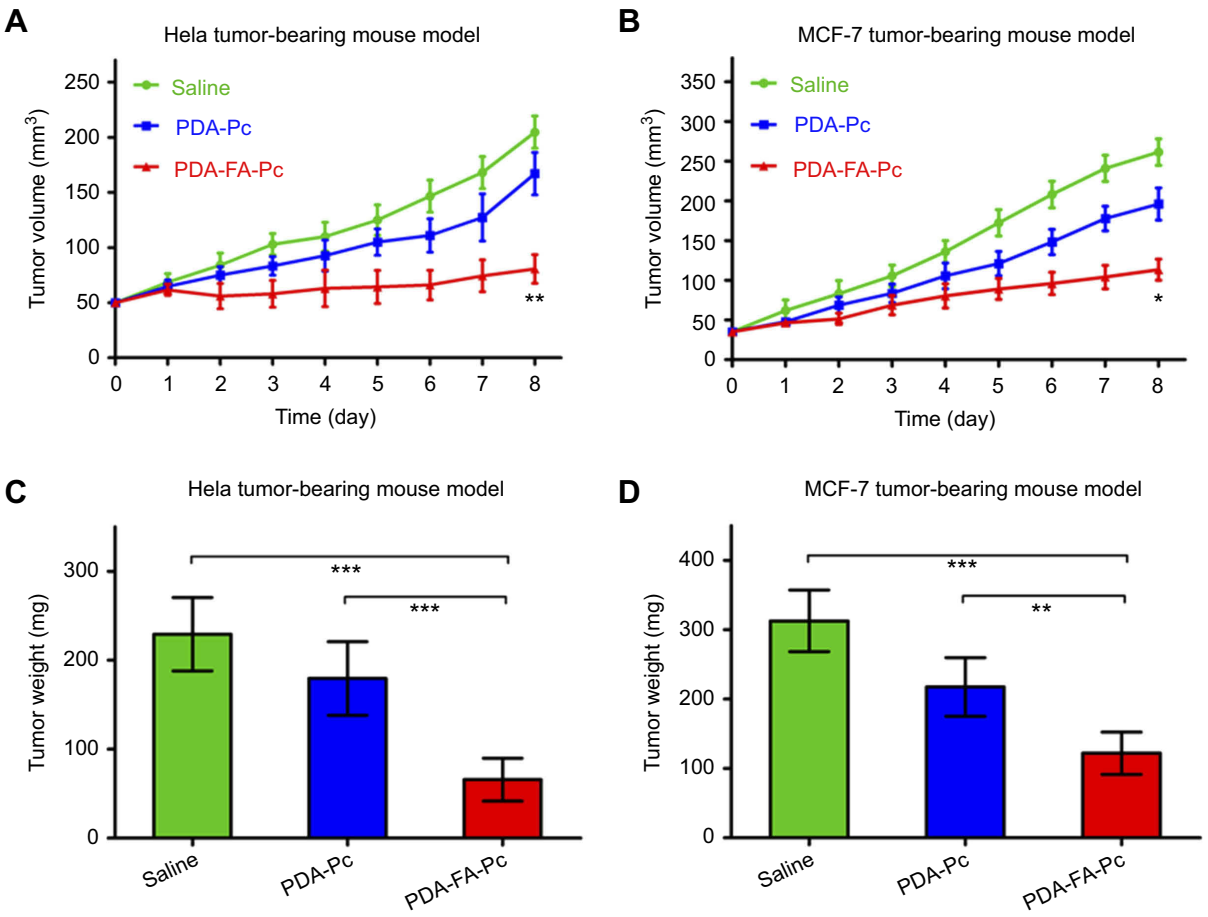

Figure 7 . In vivo antitumor efficacies of PDA-FA-Pc nanomedicine in tumor-bearing mice. (**A**,**B**) The tumor volumes in Hela tumor-bearing mice (**A**) and MCF-7 tumor-bearing mice (**B**) were daily monitored after illumination on Day 0. (**C**,**D**) The weights of tumors resected from Hela tumor-bearing mice (**C**) and MCF-7 tumor-bearing mice (**D**) on Day 8. The values were represented as mean ± SEM, ***p <0.001, **p<0.01, *p <0.05 vs the vehicle (saline-treated) group.

PDA-FA-Pc specifically target the tumor sites in cancer-grafted mice

To verify the tumor-targeting property of PDA-FA-Pc nanomedicine in vivo, we imaged the fluorescence of Pc through a noninvasive molecular tomographic imaging in MCF-7 tumor-bearing mice (Figure 6). Tumors were implanted in the right flank of the mice, and PDA-FA-Pc nanomedicine was intravenously administrated after the tumor matured (100–150 mm^3). At the time points of 3, 6, 12, 24, 48 and 96 hrs after administration, the Pc fluorescence was collected both at the tumor site in the right flank and at the non-tumor site in the symmetrical left flank (Figure 6A). The relative concentrations were quantified according to the Pc fluorescence signals (Figure 6B). At both the tumor and non-tumor sites, the accumulation of Pc kept on increasing and reached the peak at 12 hrs, which was followed by a gradual reduction till 96 hrs. At each time point, Pc accumulation at the tumor site was significantly higher than that at the non-tumor site (approximate threefold higher). In addition, no measurable Pc fluorescence was detected at either the tumor and non-tumor sites of tumor-grafted mice without PDA-FA-Pc administration (Figure 6C), indicating the stability of our data. This FMT result demonstrates that PDA-FA-Pc nanomedicine is able to specifically accumulate at tumor sites, while has very low accumulation at healthy tissues, suggesting it has excellent tumor-targeting property and high specificity.

PDA-FA-Pc nanomedicine suppressed tumor growth in human cancer-xenografted mice models

To further investigate the anticancer effects of our PDA-FA-Pc nanomedicine in vivo, we established two human cancer-xenografted mice models by subcutaneously implanting Hela and MCF-7 cells into the right flank of mice. After the tumors

reached maturity (50 mm^3 for Hela-bearing mice and 35 mm^3 for MCF-7-bearing mice), mice were intravenously administrated with PDA-FA-Pc nanomedicines (43.5 mg/kg). One group with saline administration was set as the negative control. To evaluate the role of the FA-FRs interactions on the anticancer efficacies, we also parallelly determined the antitumor effects of PDA-Pc without FA modification for comparison. Twelve hours after administration, the tumor sites were illuminated with 680 nm laser for 10 mins at the light dose of 75 J/cm^2. Tumor growth was monitored daily after illumination on day 0 by measuring the tumor volumes and the body weights. Administration with PDA-Pc and PDA-FA-Pc nanomedicine significantly suppressed the tumor growth compared to the saline administration in both models (Figure 7A and B). Particularly, PDA-FA-Pc nanomedicine administration exhibited higher antitumor effects than PDA-Pc administration did, demonstrating that the incorporation with FA enhanced the antitumor effects by targeting the pericellular FR in tumor tissues. On day 8, tumors were resected and weighed after anesthesia and sacrifice of mice (Figure 7C and D). According to the tumor weights, administration with PDA-FA-Pc nanomedicine suppressed the 71% and 62% tumor growth in Hela- and MCF-7-bearing mice, respectively. In contrast, PDA-Pc only suppressed 22% and 30% tumor growth in Hela- and MCF-7-bearing mice, respectively. The relatively mild anticancer effects of PDA-Pc might be due to the passive antitumor property of the EPR effects in the tumor sites. However, the remarkable anticancer effects of PDA-FA-Pc nanomedicine can be a result of the combination of the EPR effects and the active tumor-targeting property of the FA moiety. In addition, the body weights of the tumor-bearing mice were monitored throughout the observation window (days 0–8). Neither PDA-Pc nor PDA-FA-Pc nanomedicine showed measurable influence on body weights in contrast to the saline-treated groups (Figure S9), indicating that PDA-FA-Pc nanomedicine and its PDT treatments were reasonably well tolerated by mice.

Conclusion

In our current study, to address the metabolic problem and the off-target phototoxicities of clinical photosensitizers, we developed a receptor-targeting PDA-based carrier for the delivery of photosensitizers to tumor tissues. We used a FA-modified PDA carrier to load a highly positively charged phthalocyanine-type photosensitizer (Pc) generating the positively charged PDA-FA-Pc nanomedicine. PDA-FA-Pc nanomedicine demonstrated high stability in neutralized physiological conditions, while specifically released Pc for PDT in the acidic tumor microenvironment or lysosomes. Besides, PDA-FA-Pc nanomedicine demonstrated remarkable specificity to tumor cells as it showed remarkably higher uptake and phototoxicities in tumor cell lines (Hela and MCF-7) in contrast to those in healthy cell lines (HELF and L02). In addition, in two human cancer-xenografted mice models, PDA-FA-Pc nanomedicine significantly suppressed tumor growth and showed no obvious systemic damages. This study not only indicates that PDA-FA-Pc nanomedicine is a highly potent anticancer agent, but also suggests that using the FR-targeting PDA-based carrier is able to promote the metabolic stabilities and active tumor-targeting properties of medicinal photosensitizers for cancer treatments.

Acknowledgments

This work was financially supported by the National Natural Science Foundation of China (21708043 and 21804134), the Start-up Foundation for Advanced Talents in Sanming University (No. 18YG04), the Higher School of Applied Discipline Construction Project of Fujian Province, China (No. 44 document in 2017), the Natural Science Foundation of Fujian Province (2018J05031) and grants from the Ministry of Science and Technology (2017YFE0103200).

Disclosure

The authors report no conflicts of interest in this work.

References

1. Siegel RL, Miller KD, Jemal A. Cancer statistics, 2018. *CA Cancer J Clin*. 2018;68(1):7–30. doi:10.3322/caac.21442
2. Siegel RL, Miller KD, Fedewa SA, et al. Colorectal cancer statistics, 2017. *CA Cancer J Clin*. 2017;67(3):104–117.
3. Lin KY, Kraus WL. PARP inhibitors for cancer therapy. *Cell*. 2017;169(2):183. doi:10.1016/j.cell.2017.03.034
4. Simona M, Julien N, Patrick CJNM. Stimuli-responsive nanocarriers for drug delivery. *Nat Mater*. 2013;12(11):991–1003. doi:10.1038/nmat3776
5. Wang Y, Zhao Q, Han N, et al. Mesoporous silica nanoparticles in drug delivery and biomedical applications. *Nanomedicine*. 2015;11(2):313–327. doi:10.1016/j.nano.2014.09.014
6. Maeding N, Verwanger T, Krammer B. Boosting tumor-specific immunity using PDT. *Cancers*. 2016;8(10):91. doi:10.3390/cancers8100091
7. Castano AP, Mroz P, Hamblin MR. Photodynamic therapy and anti-tumour immunity. *Nat Rev Cancer*. 2006;6(7):535–545. doi:10.1038/nrc1894
8. Chilakamarthi U, Giribabu L. Photodynamic therapy: past, present and future. *Chem Rec*. 2017;17(8):775–802. doi:10.1002/tcr.201600121
9. Straten D, Mashayekhi V, Bruijn HS, Oliveira S, Robinson D. Oncologic photodynamic therapy: basic principles, current clinical status and future directions. *Cancers*. 2017;9(12):19. doi:10.3390/cancers9020019
10. Dabrowski JM. Reactive oxygen species in photodynamic therapy: mechanisms of their generation and potentiation. *Adv Inorg Chem*. 2017;70:343–394.
11. Dougherty TJ, Kaufman JE, Goldfarb A, Weishaupt KR, Boyle D, Mittleman A. Photoradiation therapy for the treatment of malignant tumors. *Cancer Res*. 1978;38(8):2628–2635.

12. Abrahamse H, Hamblin MR. New photosensitizers for photodynamic therapy. *Biochem J*. 2016;473(4):347–364. doi:10.1042/BJ20150942
13. Ren H, Liu J, Su F, et al. Relighting photosensitizers by synergistic integration of albumin and perfluorocarbon for enhanced photodynamic therapy. *ACS Appl Mater Interfaces*. 2017;9(4):3463–3473. doi:10.1021/acsami.6b14885
14. Voon SH, Kiew LV, Lee HB, et al. In vivo studies of nanostructure-based photosensitizers for photodynamic cancer therapy. *Small*. 2014;10(24):4993–5013. doi:10.1002/smll.201401416
15. Espinosa-Cano E, Palao-Suay R, Aguilar MR, et al. Polymeric nanoparticles for cancer therapy and bioimaging. *J Drug Target*. 2018;16(2):108–123.
16. Qin SY, Zhang AQ, Cheng SX, Rong L, Zhang XZ. Drug self-delivery systems for cancer therapy. *Biomaterials*. 2017;112:234–247. doi:10.1016/j.biomaterials.2016.10.016
17. Huo M, Wang L, Chen Y, Shi J. Tumor-selective catalytic nanomedicine by nanocatalyst delivery. *Nat Commun*. 2017;8(1):357. doi:10.1038/s41467-017-00424-8
18. Doane TL, Burda C. The unique role of nanoparticles in nanomedicine: imaging, drug delivery and therapy. *Chem Soc Rev*. 2012;41(7):2885–2911. doi:10.1039/c2cs15260f
19. Elizabeth H, Gang ZJN. Cancer nanomedicine: addressing the dark side of the enhanced permeability and retention effect. *Nanomedicine*. 2015;10(13):1993–1995. doi:10.2217/nnm.15.86
20. Uma P, Hiroshi M, Jain RK, et al. Challenges and key considerations of the enhanced permeability and retention effect for nanomedicine drug delivery in oncology. *Cancer Res*. 2013;73(8):2412–2417. doi:10.1158/0008-5472.CAN-12-4561
21. Veronese FM, Pasut G. PEGylation, successful approach to drug delivery. *Drug Discov Today*. 2005;10(21):1451–1458. doi:10.1016/S1359-6446(05)03575-0
22. Verhoef JJ, Anchordoquy TJ. Questioning the use of PEGylation for drug delivery. *Drug Deliv Transl Res*. 2013;3(6):499–503.
23. Yu G, Zhu B, Shao L, et al. Host-guest complexation-mediated codelivery of anticancer drug and photosensitizer for cancer photochemotherapy. *P Natl Acad Sci USA*. 2019;116(14):6618–6623. doi:10.1073/pnas.1902029116
24. Yu G, Cen TY, He Z, et al. Porphyrin nanocage-embedded single-molecular nanoparticles for cancer nanotheranostics. *Angew Chem Int Edit*. 2019;58(26):8799–8803. doi:10.1002/anie.201903277
25. Guo B, Zhao J, Wu C, et al. One-pot synthesis of polypyrrole nanoparticles with tunable photothermal conversion and drug loading capacity. *Colloid Surface B*. 2019;177:346–355. doi:10.1016/j.colsurfb.2019.02.016
26. Wu C, Wang S, Zhao J, et al. Biodegradable Fe(III)@WS2-PVP nanocapsules for redox reaction and TME-enhanced nanocatalytic, photothermal, and chemotherapy. *Adv Funct Mater*. 2019;29(26):1901722. doi:10.1002/adfm.201901722
27. Lynge ME, Rebecca VDW, Almar P, Brigitte SDJN. Polydopamine–a nature-inspired polymer coating for biomedical science. *Nanoscale*. 2011;3(12):4916–4928. doi:10.1039/c1nr10969c
28. Yanlan L, Kelong A, Lehui LJCR. Polydopamine and its derivative materials: synthesis and promising applications in energy, environmental, and biomedical fields. *Chem Rev*. 2014;114(9):5057–5115. doi:10.1021/cr400407a
29. Dong ZL, Gong H, Gao M, et al. Polydopamine nanoparticles as a versatile molecular loading platform to enable imaging-guided cancer combination therapy. *Theranostics*. 2016;6(7):1031–1042. doi:10.7150/thno.14431
30. Yan SF, Song XR, Liu Y, et al. An efficient synergistic cancer therapy by integrating cell cycle inhibitor and photosensitizer into polydopamine nanoparticles. *J Mater Chem B*. 2018;6(17):2620–2629. doi:10.1039/C8TB00076J
31. Wang S, Zhao X, Wang S, Qian J, He S. Biologically inspired polydopamine capped gold nanorods for drug delivery and light-mediated cancer therapy. *ACS Appl Mater Interfaces*. 2016;8(37):24368–24384. doi:10.1021/acsami.6b05907
32. Chen W, Qin M, Chen X, Wang Q, Zhang Z, Sun XJT. Combining photothermal therapy and immunotherapy against melanoma by polydopamine-coated Al2O3nanoparticles. *Theranostics*. 2018;8(8):2229–2241. doi:10.7150/thno.24073
33. Lin LS, Cong ZX, Cao JB, et al. Multifunctional Fe3O4@Polydopamine Coreâ-shell nanocomposites for intracellular mRNA detection and imaging-guided photothermal therapy. *ACS Nano*. 2014;8(4):3876. doi:10.1021/nn500722y
34. Wang C, Xu H, Liang C, et al. Iron oxide @ polypyrrole nanoparticles as a multifunctional drug carrier for remotely controlled cancer therapy with synergistic antitumor effect. *ACS Nano*. 2013;7(8):6782–6795. doi:10.1021/nn4017179
35. Ding L, Zhu X, Wang Y, et al. Intracellular fate of nanoparticles with polydopamine surface engineering and a novel strategy for exocytosis-inhibiting, lysosome impairment-based cancer therapy. *Nano Lett*. 2017;17(11):6790–6801. doi:10.1021/acs.nanolett.7b03021
36. Ge R, Lin M, Li X, et al. Cu(2+)-loaded polydopamine nanoparticles for magnetic resonance imaging-guided pH- and near-infrared-light-stimulated thermochemotherapy. *ACS Appl Mater Interfaces*. 2017;9(23):19706–19716. doi:10.1021/acsami.7b05583
37. Kurahara H, Takao S, Kuwahata T, et al. Clinical significance of folate receptor beta-expressing tumor-associated macrophages in pancreatic cancer. *Ann Surg Oncol*. 2012;19(7):2264–2271. doi:10.1245/s10434-012-2263-0
38. Teng L, Xie J, Teng L, Lee RJ. Clinical translation of folate receptor-targeted therapeutics. *Expert Opin Drug Del*. 2012;9(8):901–908. doi:10.1517/17425247.2012.694863
39. Ross JF, Chaudhuri PK, Ratnam M. Differential regulation of folate receptor isoforms in normal and malignant tissues in vivo and in established cell lines. Physiologic and clinical implications. *Cancer*. 2015;73(9):2432–2443. doi:10.1002/1097-0142(19940501)73:9<2432::AID-CNCR2820730929>3.0.CO;2-S
40. Assaraf YG, Leamon CP, Reddy JA. The folate receptor as a rational therapeutic target for personalized cancer treatment. *Drug Resist Update*. 2014;17(4–6):89–95. doi:10.1016/j.drup.2014.10.002
41. Ren D, Kratz F, Wang SW. Engineered drug-protein nanoparticle complexes for folate receptor targeting. *Biochem Eng J*. 2014;89:33–41. doi:10.1016/j.bej.2013.09.008
42. Zheng M, Gong P, Zheng C, et al. Lipid-polymer nanoparticles for folate-receptor targeting delivery of doxorubicin. *J Nanosci Nanotechnol*. 2015;15(7):4792–4798. doi:10.1166/jnn.2015.9604
43. Muller C, Schibli R. Prospects in folate receptor-targeted radionuclide therapy. *Front Oncol*. 2013;3:249. doi:10.3389/fonc.2013.00249
44. Annette K, Laura W, Laura H, et al. Targeted uptake of folic acid-functionalized iron oxide nanoparticles by ovarian cancer cells in the presence but not in the absence of serum. *Nanomedicine*. 2014;10(7):1421–1431. doi:10.1016/j.nano.2014.01.006
45. Zhang H, Li JC, Hu Y, Shen MW, Shi XY, Zhang GF. Folic acid-targeted iron oxide nanoparticles as contrast agents for magnetic resonance imaging of human ovarian cancer. *J Ovarian Res*. 2016;9(1):19. doi:10.1186/s13048-016-0230-2
46. Shakeri-Zadeh A, Kamrava SK, Farhadi M, Hajikarimi Z, Maleki S, Ahmadi A. A scientific paradigm for targeted nanophotothermolysis; the potential for nanosurgery of cancer. *Laser Med Sci*. 2014;29(2):847–853. doi:10.1007/s10103-013-1399-x
47. Beik J, Khademi S, Attaran N, et al. A nanotechnology-based strategy to increase the efficiency of cancer diagnosis and therapy: folate-conjugated gold nanoparticles. *Curr Med Chem*. 2017;24(39):4399–4416. doi:10.2174/0929867324666170810154917
48. Eyvazzadeh N, Shakeri-Zadeh A, Fekrazad R, Amini E, Ghaznavi H, Kamran Kamrava S. Gold-coated magnetic nanoparticle as a nanotheranostic agent for magnetic resonance imaging and photothermal therapy of cancer. *Laser Med Sci*. 2017;32(7):1469–1477. doi:10.1007/s10103-017-2267-x

49. Mirrahimi M, Hosseini V, Kamrava SK, et al. Selective heat generation in cancer cells using a combination of 808 nm laser irradiation and the folate-conjugated Fe2O3@Au nanocomplex. *Artif Cell Nanomed B*. 2018;46(sup1):241–253. doi:10.1080/21691401.2017.1420072
50. Neshastehriz A, Tabei M, Maleki S, Eynali S, Shakeri-Zadeh A. Photothermal therapy using folate conjugated gold nanoparticles enhances the effects of 6MV X-ray on mouth epidermal carcinoma cells. *J Photoch Photobio B*. 2017;172:52–60. doi:10.1016/j.jphotobiol.2017.05.012
51. Zeinizade E, Tabei M, Shakeri-Zadeh A, et al. Selective apoptosis induction in cancer cells using folate-conjugated gold nanoparticles and controlling the laser irradiation conditions. *Artif Cell Nanomed B*. 2018;46(sup1):1026–1038. doi:10.1080/21691401.2018.1443116
52. Movahedi MM, Mehdizadeh A, Koosha F, et al. Investigating the photo-thermo-radiosensitization effects of folate-conjugated gold nanorods on KB nasopharyngeal carcinoma cells. *Photodiagn Photodyn*. 2018;24:324–331. doi:10.1016/j.pdpdt.2018.10.016
53. Beik J, Jafariyan M, Montazerabadi A, et al. The benefits of folic acid-modified gold nanoparticles in CT-based molecular imaging: radiation dose reduction and image contrast enhancement. *Artif Cell Nanomed B*. 2018;46(8):1993–2001.
54. Ghaznavi H, Hosseini-Nami S, Kamrava SK, et al. Folic acid conjugated PEG coated gold-iron oxide core-shell nanocomplex as a potential agent for targeted photothermal therapy of cancer. *Artif Cell Nanomed B*. 2018;46(8):1594–1604.
55. Zhang Y, Zheng K, Chen Z, et al. Rapid killing of bacteria by a new type of photosensitizer. *Appl Microbiol Biotechnol*. 2017;101(11):4691–4700. doi:10.1007/s00253-017-8133-8
56. Yan SF, Chen JC, Cai LZ, et al. Phthalocyanine-based photosensitizer with tumor-pH-responsive properties for cancer theranostics. *J Mater Chem B*. 2018;6(38):6080–6088. doi:10.1039/C8TB01884G
57. Cheng W, Nie J, Xu L, et al. pH-sensitive delivery vehicle based on folic acid-conjugated polydopamine-modified mesoporous silica nanoparticles for targeted cancer therapy. *ACS Appl Mater Interfaces*. 2017;9(22):18462–18473. doi:10.1021/acsami.7b02457
58. Zhao J, Feng SS. Effects of PEG tethering chain length of vitamin E TPGS with a Herceptin-functionalized nanoparticle formulation for targeted delivery of anticancer drugs. *Biomaterials*. 2014;35(10):3340–3347. doi:10.1016/j.biomaterials.2014.01.003
59. Fuster MM, Esko JD. The sweet and sour of cancer: glycans as novel therapeutic targets. *Nat Rev Cancer*. 2005;5(7):526–542. doi:10.1038/nrc1649
60. Piscuoglio S, Ng CK, Murray MP, et al. The genomic landscape of male breast cancers. *Clin Cancer Res*. 2016;22(16):4045–4056. doi:10.1158/1078-0432.CCR-15-2840>